

Feature Extraction Based Machine Learning Approach for Bone Cancer Detection

K. Punithavathi¹ and G. Madhurasree²

¹Assistant Professor, ²PG Student,

Department of Electronics and Communication Engineering, Idhaya Engineering College for Women, Tamil Nadu, India

E-mail: punithavathikrishnamoorthy@gmail.com, madhurasreeg2000@gmail.com

(Received 5 October 2023; Revised 1 November 2023, Accepted 17 November 2023; Available online 23 November 2023)

Abstract - Osteosarcoma is a type of cancer that develops in the bones. Though it can happen in any bone, it commonly happens in long bones like the legs and arms. As a result, early detection and categorization of bone cancers have become critical for treating patients. A wavelet-based segmentation algorithm was utilized in this work to detect bone cancers. The segmented bone cancer components were then processed further for categorization. The enhanced convolutional neural network (ECNN) classification was employed in this investigation to differentiate between benign and malignant bone cancers. Collect multiple photos and use wavelet transform features to extract a trained classifier model. Sensitivity (97%), Specificity (97%), Precision (98%), Accuracy (97.5%), and F1Score (97.5) are the performance metrics for the ECNN deep learning (DL) algorithm. According to the results, ECNN deep learning beats deep learning methods, including SVM, ANN, and RNN. As a result, the ECNN deep learning technology can be used to diagnose bone cancer more accurately. Based on histology pictures, our enhanced model performs at the cutting edge of detecting osteosarcoma cancer.

Keywords: Segmentation, K-Mean, Feature Extraction, Wavelet Transform, Bone Cancer Detection, Classification, Convolutional Neural Network

I. INTRODUCTION

Cancer is the world's most hazardous disease. Cancer is formally known as a malignant tumor. It is a hereditary condition that results from unregulated cell development. Deaths can be minimized if this deadly condition is detected early [1]. Cancer is a symptom of uncontrolled cellular growth that results in the formation of a malignant tumor while also causing harm to adjacent tissues [2-4]. This form of cancer can spread and disrupt the digestive, circulatory, and neural systems, as well as produce hormones that cause the body to malfunction [5-7]. Unrestricted cell development is only sometimes damaging unless it interferes with the DNA structure. If this uncontrollable cell growth is not stopped early on, the DNA dies, forming new, unneeded cells. This mechanism culminates in cancer formation and tissue growth [8]. Cancer begins with irregular bleeding, the creation of new lumps, extended coughing, changes in cup movement, unexpected weight loss, and other symptoms. Tumors are classified as malignant or noncancerous [9]. The surgical treatment of benign (noncancerous) tumors is simple, and most benign

tumors do not recur. Unlike benign tumors, malignant (cancerous) tumors have the most prominent nucleus. Bone malignancies, also known as sarcomas, develop in muscle, fibrous tissue, bone, blood vessels, and other tissues throughout the human body. Some standard tumor forms include pleomorphic sarcoma, Chondrosarcoma, fibrosarcoma, and Ewing's sarcoma. Tumors begin to form in the bone in bone cancer, affecting bone movement and growth. A chondroma is a type of benign bone tumor that develops into cartilage. Enchondromas are most common in the ossicles of the hand. Enchondromas can develop in the upper arm, tibia, or femur [10, 11]. Bone cancer is classified into four stages based on how advanced it is.

This research analyzes neural network models to distinguish tumor and non-tumor images, including VGG-16, VGG-19[17], Dense Net-20, and ResNet-101 [16]. Consider the precision, accuracy, recall, and F1-score measurements. Compare web-based solutions to see which one performs better. The suggested method consists of four steps: (a) image processing with a median filter, (b) segmentation with a K-means clustering method, (c) feature extraction with a wavelet transform, and (d) classification with CNN.

The following are the study's primary contributions.

1. It provides K-means clustering in clinical images to segment bone cancerous lesions accurately.
2. To create a novel feature extraction module that allows the system to concentrate on the wavelet transform, which collects some essential features.
3. This work proposes an enhanced CNN algorithm for detecting malignant regions in whole-slide images of bone cancers.
4. Extensive tests on real-world datasets are utilized to validate the suggested model. According to the data, it outperforms different algorithms in segmenting malignant bone lesions with complicated backgrounds and indistinct boundaries.

The remaining part of the manuscript is structured into four sections: Section 2 discusses the manuscript's literature review. Section 3 elaborates on the proposed approach. Section 4 explains the proposed method's outcomes. Finally, Section 5 brings the text to a conclusion.

II. LITERATURE REVIEW

Thalia Yeshua *et al.*, (2023) created a 3D identification and segmentation technique for incidental bone lesions in maxillofacial CBCT scans using an automated DL algorithm. With 100% accuracy, the algorithm identified all CBCT cases as having or not having bone lesions. The system detects bone lesions on axial images with good precision (98.9%) and sensitivity (95.9%), with an average data coefficient of 83.5%. The suggested approach accurately detects and segments bone lesions in CBCT scans and can be utilized as a computing device for identifying occasional bone lesions in CBCT imagery [11].

Vlad Alexandru Georgianu *et al.*, (2022) provided findings from their study of algorithms using deep learning to detect the malignant region of bone cancers using MRI. The T1 classifier has an accuracy of 93.67% during the training step, and the T2 classifier has an accuracy of 86.67%. Both classifiers were tested and found to be 95.00% accurate. The training phase had an accuracy rate of 80.84%, and the verification phase had an accuracy rate of 80.56%. The medical model’s receiver operating characteristic (ROC) curves show that the approach is capable of class separation [12].

Xu Zhiyuan *et al.*, (2022) developed a new approach for detecting mortification rate utilizing time-series X-ray imaging. In order to overcome the sample limitation of a few images, the method generates time-series X-ray images using a generative adversarial network with short-term memory. An image-to-image translation network generates initial images to increase the data further. This improved data is a training set for a 3D CNN classification algorithm. Our method magnifies oligo bone tumor radiographs by a factor of 10, approaching the biopsy necrosis rate as the

classification result, the most advanced methodology for detecting the oligo bone tumor necrosis rate [13].

Tao Yuzhang *et al.*, (2021) proposed research that compares the efficiency of DL models with pathologists for the histological classification of bone cancers based on aggressiveness. Inception V3 and VGG-16 outperform other techniques in patch-level binary and ternary categorization. The areas under the curve for Inception V3 and VGG-16 for binary classification are 0.962 and 0.971, respectively, and the Cohen kappa scores (CKS) for ternary classification are 0.731 and 0.802, respectively [14].

Samira Masudi *et al.*, (2021) suggested characteristics for lesion classification utilizing various methods, including lesion-based mean 2D ResNet-50, lesion-based mean 3D ResNet-50, 3D ResNet-18, 2D ResNeXt-50, and an ensemble of 3D ResNet-18 and 2D ResNet-50. To that end, this paper used a 75% / 12% / 13% train / validation / test split and applied various data augmentation strategies to the training set to reduce over fitting and improve dependability. This paper exhibits 92.2% accuracy on tests in correctly diagnosing benign versus malignant bone lesions [15].

III. PROPOSED METHODOLOGY

Figure 1 depicts the workflow of the median filter and K-means pooling and wavelet transform-based bone cancer diagnose system, which includes denoising X-ray images, segmentation of afflicted portions, feature extraction, and detection of bone cancer. The research uses a publicly available dataset containing 230 MRIs of patients of various classes and descriptions. Furthermore, the most recent series contains patient MRI pictures for classification. The workflow’s detailed process specification is as follows.

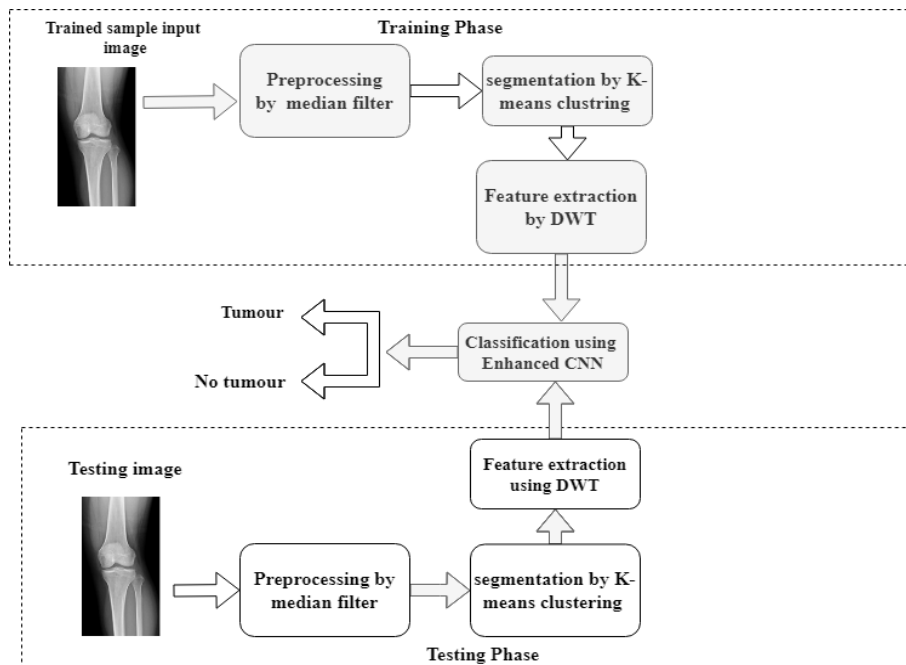


Fig. 1 Proposed Bone Cancer Detection Flow

A. Pre-Processing

The diagnosis of bone cancer begins with denoising using a median filter [16]. The acquired X-ray images contain useless information, shortening the cancer detection procedure. Then, in rank order, each pixel in the image is ranked and compared to a threshold (minimum or maximum value). If a pixel's value does not match the threshold, the noisy pixel is assumed to have been replaced using a median filter. The mean is calculated using ordered pixel values. This procedure is repeated until all noisy pixels have been successfully eliminated. Sample noise is then used to denoise X-ray pictures of bone malignancy.

B. Segmentation using K-means Clustering

The procedure is to categorize K groups based on the characteristics of the items [17]. The original image in pixels is converted to feature space (RGB) using K-means binning. Similar data points, such as with similar colors, are clustered using a clustering method to construct clusters. The method's implementation is divided into two steps. In the first stage, the centroid k is calculated, and each point is added to the cluster, with the centroid closest to the corresponding data point added in the second phase. Each group is represented by its member objects and centroid. Each cluster at the centroid accounts for the sum of all distances of the minimized items in that cluster. As a result, K-means clustering is an iterative method for decreasing the distance between each object and the cluster's centroid.

C. Feature Extraction Using Wavelet Transform

Wavelets resemble oscillations, with amplitude beginning at 0 and decreasing to zero. It combines a "multiply, reverse, integrate, and shift" procedure (known as convolution) with feature extraction from known signals to aid in the extraction of data from unknown signals. This is a numerical tool for expressing signals or images in both the spatial and frequency domains.

As a result, it renders images in a variety of resolutions. Wavelet families include Daubechies, Haar, Coiflets, biorthogonal, preserving biorthogonal, Symlets, discrete Meyer, and others. Given an image $F(X, Y)$ of size $m \times n$, whose direct discrete transformation $t(u, v, \dots)$ is given by equation (1) as,

$$t(u, v, \dots) = \sum_{X, Y} F(X, Y) g_{u, v, \dots}(X, Y) \quad (1)$$

Where X and Y represent the spatial parameters and u, v, \dots represent the transform domain parameters. With $T(u, v, \dots)$, $f(x, y)$ is able to be obtained using the IDT, as shown in the following Eqn (2).

$$F(X, Y) = \sum_{u, v, \dots} t(u, v, \dots) h_{u, v, \dots}(X, Y) \quad (2)$$

Where $g_{u, v, \dots}$ represents forward transform kernels and $h_{u, v, \dots}$ represents inverse transform kernels.

D. Classification CNN

The combined deep learning and attention mechanism model is becoming increasingly important in the era of continuous deep learning development because the attention mechanism-based neural network shows significant flexibility in learning attention, and humans may also enhance neural networks. The attention mechanism is used to understand the network. The ECNN method accomplishes the best detection effect. The attention mechanism must add another layer of weights to the image to identify the actual image's essential features using a mask, and then learn these key elements and serve the network, i.e., form attention. The model generates two sorts of attention: soft attention and hard attention.

Because the input to CNN is a color image with three RGB channels, the process of raw data by organizing it with three trainable convolution kernel filters to obtain the bottom layer of the C1 map.

After that, in S2, the ReLU activation function is utilized to execute feature processing on the convolutional picture, highlighting the image's complicated feature information and obtaining the mapping layer. The clustering kernel then selects and filters the obtained features in C3 to create the feature information map. The information graph is then analyzed in C3 and sent to the S4 layer. The pixel values in the S4 layer are then sent to various neural networks via the fully connected layer's non-spatial expansion structure to generate 1D signals.

$$U_i^j = \sum_{i \in M_j}^N x_i \times W_{i,j}^{l-1} + 2b \quad (3)$$

$$x_i = f(x) + f(U_i^j) \quad (4)$$

Euclidean distance is utilized for calculating two vectors with comprehensive data and no missing dimension data; if the measurement units between the dimensions of the two vectors are the same, this formula works fine, but if the values on the vector dimensions differ, this formula fails. A large order of magnitude necessitates normalization; otherwise, computing the difference in missing dimensions will occur. Each vector dimension is processed individually so that each dimension conforms to a conventional normal distribution. Figure 2 depicts the flow chart of the enhanced CNN.

The design of the CNN includes various hidden layers, each of which contains a large number of parameters, and the training phase of these parameters requires a large number of image data; the experience is completely learned from these large amounts of data as well as expertise in image data, such that the features retrieved by the CNN may efficiently select visual data from several layers of distinct content in the original image and undergo multi-layer nonlinear modification.

Extracted features and multi-layer nonlinear transformation have effective nonlinear transformation capabilities, allowing them to differentiate between different environmental changes, such as lighting, weather, seasons, and so on, in order to collect more sophisticated information and ensure that the features extracted have excellent invariance possesses a competitive advantage in the environment. After using the feature extraction algorithm to obtain the image's feature vector, calculate the distance between the query image and the reference image feature vector, and decide whether there is a match. The closer the

distance, the more similar the two photos, and then establish a threshold to determine the total location accuracy and other recognition algorithm parameters. The most frequent approaches for measuring sample distance in disease prediction and classification research include Euclidean distance, Manhattan distance, cosine distance, and so on.

$$\text{Manhattan_dist} = \sum_{i=1}^n |y_i^2 - x_i^2| \sqrt{2} \quad (5)$$

$$f_{ma}(v) = y^2 - \max_{1 < M \leq t} v_M \quad (6)$$

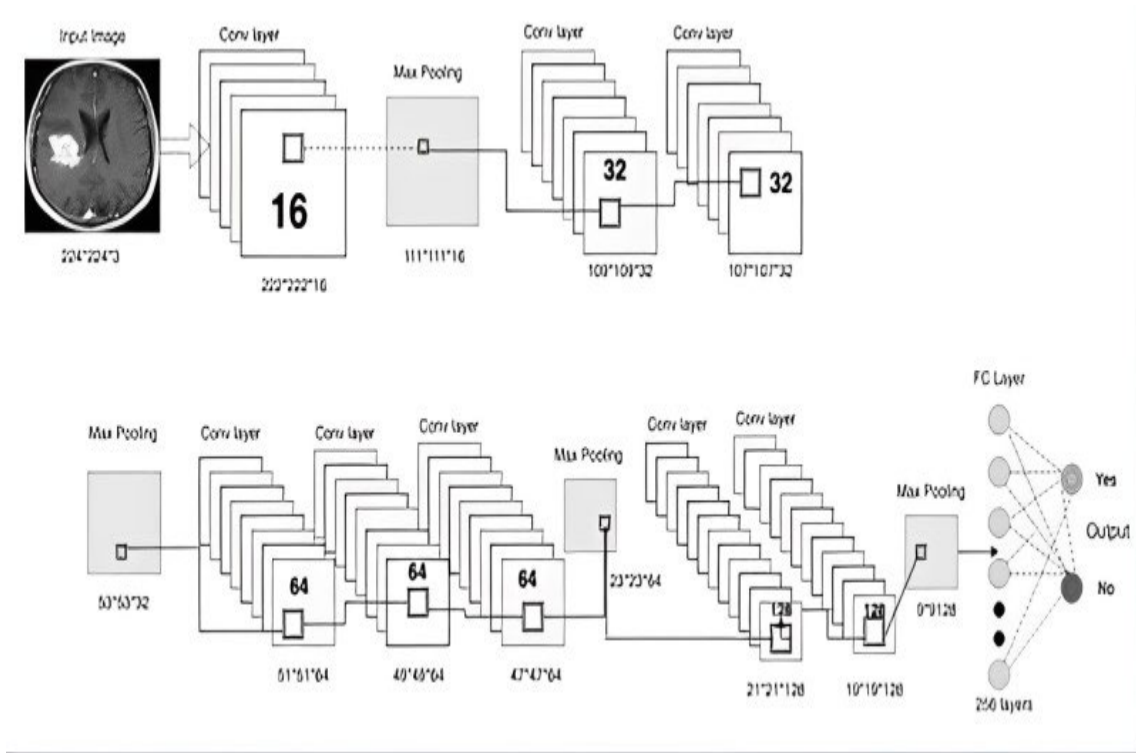


Fig. 2 Enhanced Convolutional Neural Network Enhances Model

IV. RESULTS AND DISCUSSION

Table I depicts the outcomes of assessing parameters like accuracy, sensitivity, precision, F1score, and specificity after executing the proposed work on publicly available datasets.

A. Performance Parameters

Model evaluation parameters:

F1 score is the weighted average of the model's sensitivity and precision. These are more reliable than accuracy.

$$F1 \text{ score} = 2 \cdot \frac{\text{Sensitivity} \cdot \text{Precision}}{\text{Sensitivity} + \text{Precision}}$$

Accuracy is a minor component of correct prediction devised by every model concerning total prophecy in each instance.

$$\text{Accuracy} = \frac{T(+)+T(-)}{T(+)+T(-)+F(+)+F(-)}$$

Precision is a part of the correct hopeful prophecy concerning all outstanding optimistic dignity. A high score means fewer incorrect predictions.

$$\text{Precision} = \frac{T(+)}{T(+)+F(+)}$$

Sensitivity is the percentage of relevant occurrences that are recovered.

$$\text{Sensitivity} = \frac{T(+)}{T(+)+F(-)}$$

Specificity indicates the ratio of correct non-ROI region segmentation.

$$\text{Specificity} = \frac{T(-)}{T(-)+F(+)}$$

Where,

T(+): True positive is the number of pixels accurately segregated as ROI region.

T(-): True Negative is the number of pixels accurately segregated as the non-ROI region.

F(+): False positive is the number of pixels wrongly categorized into ROI region.

F(-): False Negative is the number of pixels improperly categorized as the non-ROI region.

TABLE I BONE CANCER DETECTION AND CLASSIFICATION EFFICACY

Models	Accuracy	Specificity	Precision	Sensitivity	F1-score
SVM	89	87	91	92	90.6
CNN	93.5	92.6	92.5	93.5	93.5
RNN	95	94.5	95	96	95.8
Proposed	97.5	97	98	97	97.5

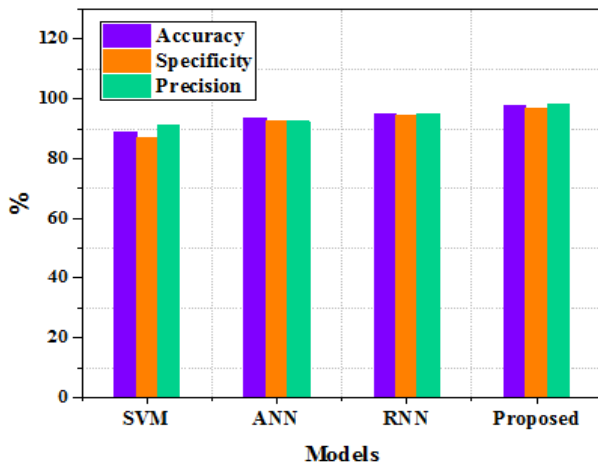


Fig. 3 Performance metrics comparison (Accuracy, Specificity and precision)

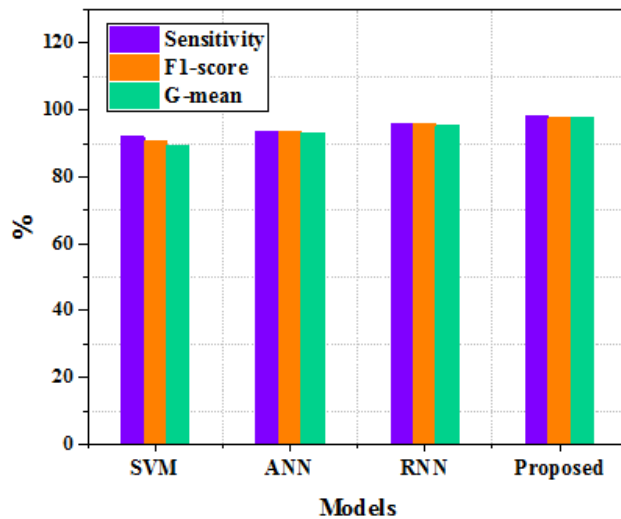


Fig. 4 Performance metrics comparison (Sensitivity, F1 score and G-mean)

Table I displays the total scores of all methods in the dataset. Figures 3 and 4 shows that the results achieved by all of the models are satisfactory. The proposed system employs supervised deep-learning approaches for model training. SVM, CNN, RsNet-50 methods also solve classification problems. The accuracy of the SVM model was 89%, the specificity was 87%, the precision was 91%, the sensitivity

was 92%, and the F1 score was 90.6%, which was average compared to other models. The accuracy of the ANN model was 93.5%, the specificity was 92.6%, the precision was 92.5%, the sensitivity was 93.5%, and the F1 score was 93.5%. The accuracy of the RNN model is 95%, the specificity is 94.5%, the precision is 95%, the sensitivity is 96%, and the F1 score is 95.8%. The proposed enhanced CNN model's accuracy is 97.5%, specificity is 97%, precision is 98%, sensitivity is 97%, and F1 score is 97.5%, which is the greatest compared to other models.

B. Computational Time

Table II shows the average time required by various algorithms. Most techniques, as shown in the table, take a lengthy time to calculate the actual results, such as SVM, ANN, and RNN, which take 35, 27, and 22 ms, respectively, whereas our proposed algorithm, ECNN, only takes 18ms. Figure 4 depicts the graphical representation of computational time.

TABLE II COMPARISON OF COMPUTATIONAL TIME (MS)

Methods	Computational Time (ms)
SVM	35
ANN	27
RNN	22
Proposed	18

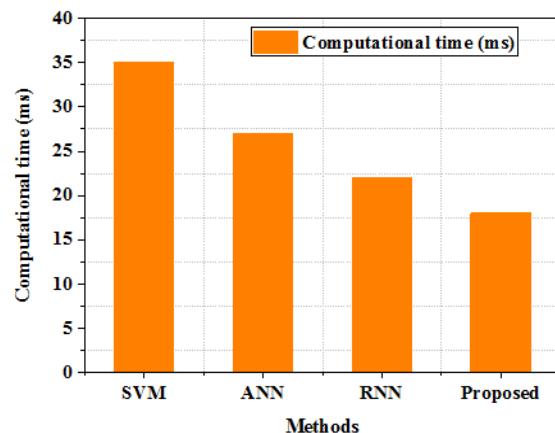


Fig. 5 Computational Time Graph

V. CONCLUSION

This work entails detecting malignancies from bone MRIs utilizing wavelet transform for feature extraction and categorizing discovered cancers as benign or malignant using ECNN. The proposed strategy emphasizes the ECNN classifier's potential for bone cancer classification. This approach is regarded as a reliable classification algorithm with high performance. Using wavelet transform and deep learning classifier classification functions, we improved performance accuracy using ECNN. ECNN with deep learning produced the most outstanding results, with Sensitivity (97%), Specificity (97%), Precision (98%), Accuracy (97.5%), and F1Score (97.5). The findings demonstrate that preprocessing delivers superior results. The results also show that the ECNN refining tool is more resilient than manual feature extraction procedures.

REFERENCES

- [1] Binhsan, "Enchondroma Tumor Detection," *International Journal of Advanced Research in Computer and Communication Engineering*, Vol. 4, No. 6, pp. 1-4, June 2015.
- [2] R. S. Savage and Y. Yuan, "Predicting Chemo insensitivity in breast cancer with omics/digital pathology data fusion," *Royal Society Open Science*, Vol. 3, No. 2, pp. 140-501, 2016.
- [3] A. Madabhushi and G. Lee, "Image analysis and machine learning in digital pathology: challenges and opportunities," *Medical Image Analysis*, Vol. 33, No. 2, pp. 170-175, 2016.
- [4] L. Xiang, Y. Qiao, D. Nie, L. An, Q. Wang and D. Shen, "Deep auto-context convolutional neural networks for standard-dose PET image estimation from low-dose PET/MRI," *Neurocomputing*, Vol. 267, No. 1, pp. 406-416, 2017.
- [5] Deepshikha Shrivastava, Sugata Sanyal, Arnab Kumar Maji and Debdatta Kandar, "Bone cancer detection using machine learning techniques," *Smart Healthcare for Disease Diagnosis and Prevention*, Academic Press, pp. 175-183, 2020. DOI:10.1016/B978-0-12-817913-0.00017-1
- [6] R. V. Santosh Singh and Y. Singh, "An evaluation of features extraction from lung CT images for the classification stage of malignancy," *IOSR Journal of Computer Engineering (IOSR-JCE)*, Vol. 9, No. 2, pp. 76-79, 2016.
- [7] A. Mishra and M. V. Suhas, "Classification of benign and malignant bone lesions on CT images using random forest," *IEEE International Conference on Recent Trends in Electronics Information Communication Technology*, Bangalore, India, pp. 1807-1810, 2016.
- [8] R. Aishwariya, M. Kalaiselvi Geetha and M. Archana, "Computer aided fracture detection of X-ray images," *IOSR Journal of Computer Engineering (IOSR-JCE)*, Vol. 1, No. 1, pp. 44-51, 2008.
- [9] G. Chu, P. Ramakrishna, H. Kim, D. Morris, J. Goldin, M. Brown, "Bone tumor segmentation on bone scans using information and random forest," *International Innovative Research Journal of Engineering and Technology (IIRJET)*, Vol. 17, No. 1, pp. 601-608, 2014.
- [10] Cem M. Deniz and S. Xiang, "Segmentation of proximal femur from MR image using deep convolution neural network," *IEEE Trans. Magn. Reson. Med.* Vol. 2, No. 1, 2017, pp. 1-26.
- [11] T. Yeshua, S. Ladyzhensky, A. Abu-Nasser, et al., "Deep learning for detection and 3D segmentation of maxillofacial bone lesions in cone beam CT," *European Radiology*, Vol. 33, pp. 7507-7518, 2023, DOI: <https://doi.org/10.1007/s00330-023-09726-6>.
- [12] V. A. Georgeanu, M. Mămuleanu, S. Ghiea and D. Selișteanu, "Malignant Bone Tumors Diagnosis Using Magnetic Resonance Imaging Based on Deep Learning Algorithms," *Medicina*, Vol. 58, No. 5, pp. 636, 2022. <https://doi.org/10.3390/medicina58050636>.
- [13] Zhiyuan Xu, Kai Niu, Shun Tang, Tianqi Song, Yue Rong, Wei Guo, Zhiqiang He, "Bone tumor necrosis rate detection in few-shot X-rays based on deep learning," *Computerized Medical Imaging and Graphics*, Vol. 102, 2022, DOI: <https://doi.org/10.1016/j.compmedimag.2022.102141>.
- [14] Tao Yuzhang, Huang Xiao, Tan Yiwen, Wang Hongwei, Jiang Weiqian, Chen Yu, Wang Chenglong, Luo Jing, Liu Zhi, Gao Kangrong, Yang Wu, Guo Minkang, Tang Boyu, Zhou Aiguo, Yao Mengli, Chen Tingmei, Cao Youde, Luo Chengsi, Zhang Jian, "Qualitative Histopathological Classification of Primary Bone Tumors Using Deep Learning: A Pilot Study," *Frontiers in Oncology*, 2021, DOI: 10.3389/fonc.2021.735739.
- [15] Samira Masoudi, Sherif Mehralivand, Stephanie A. Harmon, Nathan Lay, Liza Lindenberg, Esther Mena, Peter A. Pinto, Deborah E. Citrin, James L. Gulley, Bradford J. Wood, William L. Dahut, Ravi A. Madan, Ulas Bagci, Peter L. Choyke, Baris Turkbey, "Deep Learning Based Staging of Bone Lesions From Computed Tomography Scans," in *IEEE Access*, Vol. 9, pp. 87531-87542, 2021, DOI: 10.1109/ACCESS.2021.3074051.
- [16] Torki Altameem, Fuzzy rank correlation-based segmentation method and deep neural network for bone cancer identification. *Neural Computing and Applications*, Vol. 32, pp. 805-815, 2020, DOI: <https://doi.org/10.1007/s00521-018-04005-8>.
- [17] Rinisha Bagaria, Sulochana Wadhvani and Arun Kumar Wadhwan, "A Wavelet Transform and Neural Network Based Segmentation and Classification System For Bone Fracture Detection," *Optik*, Vol. 236, July 2021, DOI: <https://doi.org/10.1016/j.ijleo.2021.166687>.